

# A DEM Simulation on Irregular-shaped Intruders Moving in Granular Media

Mingrui Dong<sup>1,\*</sup>, Deheng Wei<sup>1,2,\*\*</sup>, and Yixiang Gan<sup>1,\*\*\*</sup>

<sup>1</sup>School of Civil Engineering, The University of Sydney, Sydney, Australia

<sup>2</sup>School of Resources and Civil Engineering, Northeastern University, Shenyang, China

**Abstract.** An intruder moving in a granular medium is a common phenomenon in nature and plays a crucial role in a wide range of industrial processes. Although regular-shaped intruders, such as spheres, ellipsoids, and cylinders, have been extensively studied, the behaviour of irregular-shaped intruders remains poorly understood. In this study, we employ the Discrete Element Method (DEM) to investigate the drag force acting on an irregular intruder moving in a granular bed consisting of spherical particles. The intruder's morphological irregularity is constructed using spherical harmonics and is controlled by two shape parameters: fractal dimension ( $D_f$ ) and relative roughness ( $R_r$ ). Our results indicate that the influence of shape on drag forces is limited in the quasi-static regime where the intruder moves at relatively low velocities. At higher velocities, however, the drag force exhibits a quadratic relationship with velocity for irregular-shaped intruders, similar to that observed for spherical ones. Notably, the prefactor in this relationship is more strongly influenced by  $R_r$  than by  $D_f$ , highlighting the dominant role of surface roughness in the inertial regime.

## 1 Introduction

An intruder moving within the granular media is a frequently observed phenomenon in nature and holds significant importance across a broad spectrum of industrial applications, such as segregation during granular handling and riverbed sedimentation. The drag force ( $F_d$ ) on the intruder depends on various factors, e.g., velocity of the intruder, the size ratio between the intruder and surrounding particles, intruder shape, granular bed solid fraction and inter-particle contact properties. At extremely low velocities ( $v_i$ ),  $F_d$  can be found nearly independent of velocities until it reaches a regime where  $F_d$  is linearly correlated to  $v_i$  [1, 2]. When further increasing the velocity, a quadratic  $F_d$ - $v_i$  relation can be found [3]. Higher solid fraction, inter-particle friction and bed overburden pressure can result in higher  $F_d$  [1, 3, 4]. Non-dimensional numbers, e.g., Froude and Inertial numbers, are widely applied to evaluate the competing effects of granular mass, velocities, and over-burden pressure [1, 5].

Although extensive research has been conducted on intruders with regular shapes, such as spheres and disks [1, 3], ellipsoids [6], cylinders [4], and their mixtures [2], understanding of irregularly shaped intruders remains relatively limited. A dimensionless number  $C_d$  is commonly adopted to evaluate the effect of the shape and effect of the intruder-particle size ratio on  $F_d$  [5, 7].

This study applies the Discrete Element Method (DEM) to investigate the drag force on an irregular intruder moving in a granular bed assembled by spherical

particles. The morphological irregularity is constructed using spherical harmonics and is controlled by two shape parameters, namely fractal dimension and relative roughness. The effect of intruder shape factors on the relation between  $F_d$  and its moving velocities ( $v_i$ ) can be characterised using two fitting functions and a drag coefficient-Froude number,  $C_d$ - $F_r$  relation. Both reflect quasi-static and dynamic states.

## 2 Method

### 2.1 Model setup

The model setup of an intruder and a granular bed is illustrated in Figure 1. Spherical particles with diameter  $d_p = 4 \text{ mm} \pm 5\%$  were poured into a simulation domain with periodic boundaries in the  $x$ - and  $y$ -directions. An initial compression (1 kPa) was applied along the  $z$ -axis until it reached a steady state, after which the particles in the bottom and top layers were fixed to form a non-slip condition and a volume-controlled bed. A solid fraction ( $\phi$ ) of 0.59 is measured in the bed with a final dimension of  $60d_p \times 50d_p \times 30d_p$  as shown in Figure 1. Then, an intruder is embedded at the mid-height of the bed and overlapping particles are removed. This setup ensures a consistent granular bed for all intruder cases, aiming to minimise the effect of different granular structures. The gravity of 9.81 m/s is applied in the negative direction of  $z$ -axis.

The morphological irregularity is constructed using spherical harmonics, which can effectively define and control single-grain morphological properties, e.g., shape and texture [8]. The morphology adopted in this study is controlled by two shape parameters, namely the fractal dimen-

\*e-mail: mingrui.dong@sydney.edu.au

\*\*e-mail: deheng.wei@sydney.edu.au

\*\*\*e-mail: yixiang.gan@sydney.edu.au

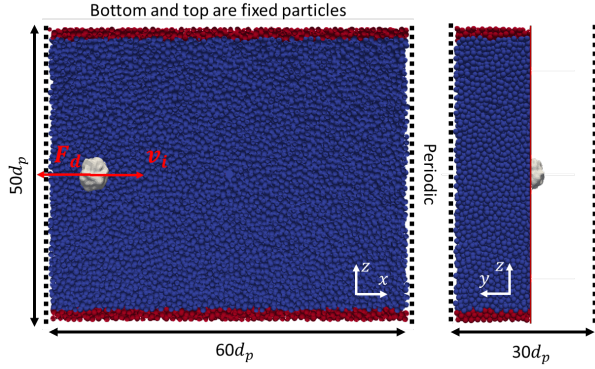


**Figure 1.** The DEM model illustration of simulation setups. An irregular-shaped intruder moves at a constant velocity  $v_i$  in the granular media, which causes a drag force  $F_d$  on the intruder. Periodic boundary conditions are applied along the  $x$ - and  $y$ -directions. Two-layers of particles are fixed at the top and bottom.

sion ( $D_f$ ) and the relative roughness ( $R_r$ ), which is illustrated in Figure 2. Note that all irregular-shaped intruders possess an equivalent volume size, the same as the spherical intruder. A mesh sensitivity study was carried out to determine the intruder mesh size as  $0.1d_p$ .

## 2.2 Inter-particle force

The DEM model is established using the open-source platform LIGGGHTS [9]. The movement of each particle is calculated via Newton's second law of motion. The normal, tangential and rolling inter-particle contact laws are shown as [10–12]:

$$F_n = k_n \delta_n - \beta_n v_n, \quad F_t = k_t \delta_t - \beta_t v_t, \quad M_r = k_r \Delta \theta_r - \beta_r \omega, \quad (1)$$

where  $n$ ,  $t$  and  $r$  represent the normal, tangential and rolling,  $F$  is the contact force,  $k$  is the contact stiffness,  $M$  is the rolling torque,  $\delta$  is the overlap distance of each pair of contacting particles,  $\Delta \theta_r$  is the relative rotation angle of contacting particles,  $\beta$  is the damping coefficient,  $v$  and  $\omega$  is the relative translational velocity and relative angular velocity for each contact pair, respectively. The tangential friction and rolling effect,  $F_t$  and  $M_r$ , adopt the Coulomb style criteria giving  $|F_t| \leq \mu_s |F_n^{\text{total}}|$  and  $|M_r| \leq \mu_r r F_n^{\text{total}}$  where  $\mu_s$  is the sliding friction coefficient and  $\mu_r$  is the rolling friction coefficient,  $r$  is the radius of particles. The computational stability and physical meaningfulness are ensured by setting the integration time step as  $t = 10^{-7} s < \sqrt{m/Ed_p}$ , where  $m$  is the mass of the average particle size,  $E$  is Young's modulus. Please see table 1 for the parameter value adopted.

## 3 Results and discussions

### 3.1 Intruder velocity

We first examine the  $F_d$  evolution when the intruder moves through the granular bed. Figure 3(a) presents three sets

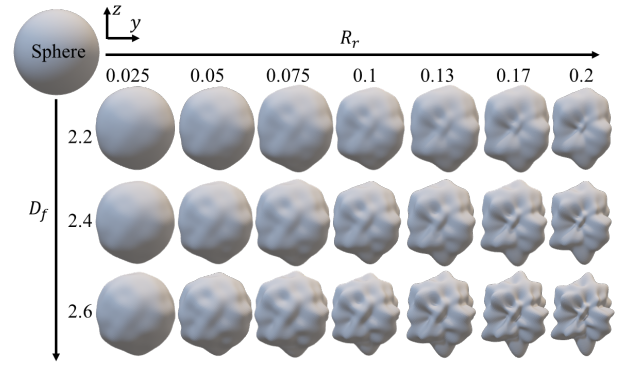


**Figure 2.** The illustration of irregular-shaped intruder characterised by  $D_f$  and  $R_r$ . The plane from the inside out points in the positive direction of the  $x$ -axis.

**Table 1.** Materials properties and parameters

Properties	Value
Young's modulus, $E$ (Pa)	$10^{10}$
Coefficient of sliding friction, $\mu_s$ (-)	0.5
Coefficient of rolling friction, $\mu_r$ (-)	0.01
Coefficient of restitution (-)	0.9
Gravitational acceleration, $g$ ( $m/s^2$ )	9.81
Particle density, $\rho$ ( $kg/m^3$ )	2460
Average particle diameter, $d_p$ (mm)	4
Equivalent intruder diameter, $D$ (mm)	$5d_p$
Intruder mesh size (mm)	$0.1d_p$
Initial bed solid fraction, $\phi$ (-)	0.59
Intruder moving velocities, $v_i$ (m/s)	0.01, 0.1, 0.2, 0.3, 0.5, 0.7, 1, 2, 3, 5, 7, 10

of  $F_d$  variation when intruders move at speeds 0.1, 1 and 3 m/s. An irregular-shaped intruder ( $D_f = 2.6$ ,  $R_r = 0.2$ ) always shows a higher  $F_d$  than a spherical intruder in each set. For the low-velocity case (0.1 m/s),  $F_d$  is nearly consistent throughout the moving period. However, a yield-like peak can be found for  $v_i = 1$  and 2 m/s during the early stage when the intruder starts to move, which are also observed in high-velocity conditions by previous studies [3, 13]. We average  $F_d$  within a steady-state sampling window to obtain  $\bar{F}_d$ , as shown in Figure 3(a), to investigate the morphological effect on the relation between  $\bar{F}_d$  and  $v_i$ .

Our results show that, for all intruders,  $\bar{F}_d$  exhibits both linear and quadratic regimes corresponding to low and high  $v_i$ , and the transition in the  $\bar{F}_d$ - $v_i$  relationship has also been observed in previous studies [1, 3]. As shown in Figure 3(b), the linear range spans from  $v_i = 0.01$  m/s to around 1 m/s, above which the trend transitions to the quadratic state. This transition can be explained as a change from a quasi-static state to an inertial state.  $F_d$  is mainly formed by long-term friction contacts between the intruder and the particle in the quasi-static state, whereas short-term collisional contacts dominate in the inertial state [1].

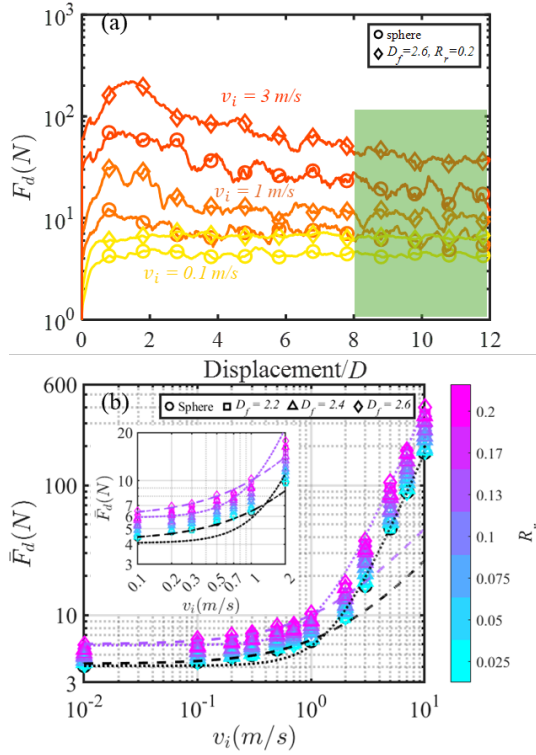


**Figure 3.** (a) Drag force  $F_d$  evolution along the intruders displacement. The  $F_d$  of three speeds of the sphere and an irregular-shaped intruder are taken as examples. The green shaded area shows where the steady state  $F_d$  is averaged. (b)  $\bar{F}_d$  as a function of  $v_i$ . Markers and colours represent the variation of  $D_f$  and  $R_r$ . Dashed and dotted lines represent fitting equations Eq.(2) and Eq.(3), where black lines indicate sphere and purple the intruder with shape factor  $D_f = 2.6$  and  $R_r = 0.2$ . Inset zooms in the range from  $v_i = 0.1$  to  $2$  m/s

### 3.2 Intruder shape

The effect of irregular shape is reflected in the increased  $\bar{F}_d$  with the increase in shape factors, especially for  $R_r$ , in all  $v_i$  cases. Two fitting functions are used to examine the detailed shape effect in the relation between  $\bar{F}_d$  and  $v_i$  in the linear and the quadratic states, which are expressed as:

$$\bar{F}_d \propto \bar{F}_0 + \alpha_1 v_i, \quad (2)$$

$$\bar{F}_d \propto \bar{F}_0 + \alpha_2 v_i^2, \quad (3)$$

where  $\bar{F}_0$  is the minimum  $\bar{F}_d$  of each intruder shape at  $v_i = 0.01$  m/s,  $\alpha_1$  and  $\alpha_2$  are fitting parameters. Figure 3(b) shows a combination of plots of simulation results (symbols) and fitting functions (lines). A good match is observed between the symbols and lines for Eq.(2) in the linear regime and for Eq.(3) in the quadratic regime, however the opposite does not hold (see the inset in Figure 3(b)). Note that the goodness-of-fit index in all fittings is  $R^2 > 0.98$ , further signalling that the two functions can effectively describe the  $\bar{F}_d - v_i$  relationship when considering the shape effect.

The fitting parameters  $\alpha_1$  and  $\alpha_2$  for different  $D_f$  are plotted against  $R_r$  as shown in Figure 4. As can be seen,

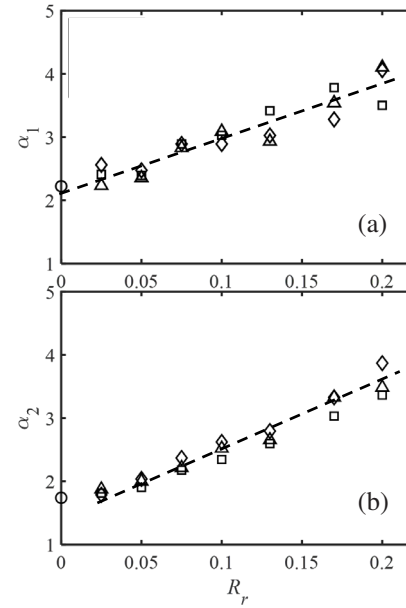


**Figure 4.** Fitting parameters  $\alpha_1$  (a) in Eq.(2) and  $\alpha_2$  (b) in Eq.(3) as the function of  $R_r$ . Symbols are the same as Figure 3(b), Dashed lines are for the guide of eyes.

$D_f$  shows limited effects on  $\alpha_1$  and  $\alpha_2$ , indicating that  $F_d$  is not sensitive to  $D_f$ . Linear trends can be observed in both the  $\alpha_1 - R_r$  and  $\alpha_2 - R_r$  relationships, signalling  $\bar{F}_d$  is mainly affected by  $R_r$  when both factors are controlled.

### 3.3 Drag coefficient

The drag coefficient  $C_d = \bar{F}_d / (0.5\rho\phi v_i^2 A_p)$ [7] and the Froude number  $F_r = 2v_i / \sqrt{gR}$ [1] are adopted to investigate the shape effects in different velocity states. Here,  $A_p$  is the projection area of intruders in the  $y-z$  plane, perpendicular to the moving direction (see the intruder morphology illustrations in Figure 2).  $R = 2.5d_p$  is the equivalent volume radius of intruders. Figure 5 shows that the relation between  $C_d$  and  $F_r$  shows a decreasing linear trend at low  $F_r$  and transitions to a plateau when above  $F_r \approx 10$ . This transition reflects comparable mechanisms (a transition from a frictional viscous regime to a turbulent inertial regime) in an object experiencing drag in a fluid or a fluidised granular media [5, 14].

Although Eq.(2) provides a good prediction based on shape-related prefactors, the collapsed  $C_d$  in the range below  $F_r \approx 10$  indicates a relatively limited shape effect in the quasi-static state. Normalising the projection area  $A_p$  in  $C_d$  indicates that  $A_p$  dominates the formation of  $F_d$ . Whilst the shape factors are effective in the inertial state, resulting in a higher  $C_d$  under the same  $F_r$  (see the inset in Figure 5). Extracting local information can help us better understand the underlying physics.

## 4 Conclusions

In this study, we applied the DEM method to investigate the drag force  $F_d$  on irregular-shaped intruders

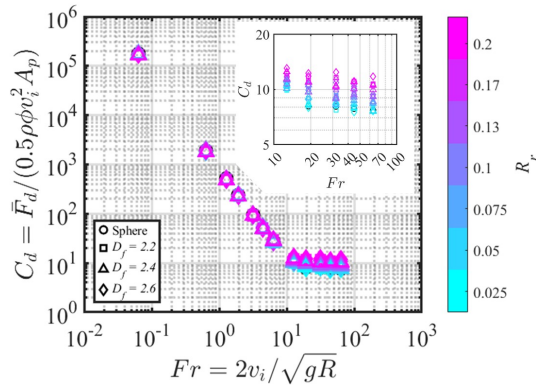


**Figure 5.** The drag coefficient versus Froude number. Inset zooms in the range from  $Fr = 10$  to  $100$ . See Figure 3(b) for explanations of markers and colours.

moving at various constant velocities in a granular bed. The irregularities of the intruder shapes are defined and controlled using the fractal dimension ( $D_f$ ) and relative roughness ( $R_r$ ). Our model obtains the linear increase in the drag force of all intruders as the velocity ( $v_i$ ) increases from  $0.01\text{ m/s}$ , and it transitions to a quadratic rise at  $v_i \approx 1\text{ m/s}$ , indicating the transition from a quasi-static regime to an inertial regime. Two fitting functions are applied to capture the two states successfully, and the fitting parameters show a linear correlation with  $R_r$ , indicating a strong correlation with the shape factor  $R_r$ . The relation between the drag coefficient ( $C_d$ ) and the Froude number ( $Fr$ ) implies comparable mechanisms in our models with those of objects moving in fluids or fluidised granular media and shows that the shape effect is more effective in the inertial state. This study enhances our understanding of the drag on morphologically irregular intruders in granular media, with potential applications across various industrial processes.

## References

- [1] J. Hilton, A. Tordesillas, Drag force on a spherical intruder in a granular bed at low froude number, *Physical Review E—Statistical, Nonlinear, and Soft Matter Physics* **88**, 062203 (2013).
- [2] A. Seguin, Forces on an intruder combining translation and rotation in granular media, *Physical Review Fluids* **7**, 034302 (2022).
- [3] Y. Takehara, K. Okumura, High-velocity drag friction in granular media near the jamming point, *Physical review letters* **112**, 148001 (2014).
- [4] F. Guillard, Y. Forterre, O. Pouliquen, Depth-independent drag force induced by stirring in granular media, *Physical review letters* **110**, 138303 (2013).
- [5] L. Jing, J.M. Ottino, P.B. Umbanhowar, R.M. Lueptow, Drag force in granular shear flows: regimes, scaling laws and implications for segregation, *Journal of Fluid Mechanics* **948**, A24 (2022).
- [6] B.K. Tripura, S. Kumar, K. Anki Reddy, J. Talbot, Role of shape on the forces on an intruder moving through a dense granular medium, *Particulate Science and Technology* **40**, 651 (2022).
- [7] J.F. Boudet, H. Kellay, Drag coefficient for a circular obstacle in a quasi-two-dimensional dilute supersonic granular flow, *Physical review letters* **105**, 104501 (2010).
- [8] D. Wei, J. Wang, J. Nie, B. Zhou, Generation of realistic sand particles with fractal nature using an improved spherical harmonic analysis, *Computers and Geotechnics* **104**, 1 (2018).
- [9] C. Kloss, C. Goniva, A. Hager, S. Amberger, S. Pirker, Models, algorithms and validation for opensource dem and cfd-dem, *Progress in Computational Fluid Dynamics, an International Journal* **12**, 140 (2012).
- [10] N.V. Brilliantov, F. Spahn, J.M. Hertzsch, T. Pöschel, Model for collisions in granular gases, *Physical review E* **53**, 5382 (1996).
- [11] K. Iwashita, M. Oda, Rolling resistance at contacts in simulation of shear band development by dem, *Journal of engineering mechanics* **124**, 285 (1998).
- [12] J. Ai, J.F. Chen, J.M. Rotter, J.Y. Ooi, Assessment of rolling resistance models in discrete element simulations, *Powder Technology* **206**, 269 (2011).
- [13] S. Athani, P. Rognon, Inertial drag in granular media, *Physical Review Fluids* **4**, 124302 (2019).
- [14] Á. Vergara, D. Wei, R. Fuentes, Drag coefficient for irregularly shaped grains: rotational dependence at various reynolds numbers, *Journal of Fluid Mechanics* **994**, A1 (2024).